Aerosol and Air Quality Research, 11: 140–154, 2011

ISSN: 1680-8584 print / 2071-1409 online
doi: 10.4209/aaqr.2010.08.0071

Experimental Study of the Effects of Environmental and Fog Condensation Nuclei Parameters on the Rate of Fog Formation and Dissipation Using a New Laboratory Scale Fog Generation Facility

Vivek Pratap Singh[1], Tarun Gupta[1*], Sachchida Nand Tripathi[1*], Chinmay Jariwala[1], Utpal Das[2]

[1] *Environmental Engineering and Management Programme, Department of Civil Engineering, Indian Institute of Technology Kanpur, India*
[2] *Department of Electrical engineering, Indian Institute of Technology Kanpur, India*

ABSTRACT

The IIT Kanpur Fog Chamber Facility has been conceptualized and built indigenously to study the fog formation and dissipation under various environmental conditions. The chamber has been designed such that all governing parameters can be controlled and optimized. The effects of relative humidity, temperature and size distribution, number and chemical composition of fog condensation nuclei (FCN) on the formation, stability and dissipation of fog has been studied. The visibility measurements were carried out using a He-Ne 632.8 nm monochromatic laser. It was found that aerosol number concentration, size distribution and chemical nature of FCN have significant effects on visibility reduction in fog. Direct comparisons were made for theoretical droplet growth and settling times in predicting the period for which stable fog was expected Vs the actual experimentally measured times for stable fog generated using different types of FCN. Effective radius, R_{eff}, of fog droplet size distribution (DSD), a parameter that describes the optical properties of the droplet distribution was also calculated. It was noted that even for the same R_{eff} (i.e. similar visibility), DSDs show notable differences depending on other conditions, implying the differences in the microphysical nature of fog. Fog dissipation results show that, with the decrease in temperature, the rate of fog dissipation decreases for all FCNs except for uncoated graphite, where no particular pattern has been observed maybe due to its less hygroscopic nature. The results from this study will help us in better understanding the optical nature of fog and designing of future fog vision devices.

Keywords*:* Fog; Condensation; Visibility; Hygroscopic; Droplet growth.

INTRODUCTION

Atmospheric fog is a weather phenomenon wherein tiny water droplets suspended in the vicinity of the earth's surface cause a reduction in visibility. The poor visibility leads to severe disruption and delay in rail, road and air traffic, causing great economic loss (Mohan and Payra, 2009). As the occurrence of fog in northern India and around the world have become more frequent in recent times, it is necessary to have detailed information about the optical nature of fog particulate system (water droplet + fog condensation nuclei), leading to poor visibility. Atmospheric fog is typically composed of sub-micron size inactivated particles associated with activated droplets of size range up to tens of micron (Pinnick *et al*., 1978; Hudson, 1980; Gerber, 1981; Frank *et al*., 1998). In order to understand the formation of fog and its effect on visibility it is important to characterize and investigate the behaviour of fog formation by identifying and understanding the size and characteristics of the most critical Fog Condensation Nuclei (FCN), responsible for dense fog formation (Bott, 1991; Yuskiewicz, 1998; Baumer, 2008). One can then find techniques to safeguard against these FCN by reducing their emissions.

There are several similar installations in different parts of the world which are using artificial fog production techniques. These facilities are available at Clermont – Ferrand laboratory, France; Leipzig Aerosol Cloud Interaction Simulator (LACIS) at Leibniz Institute for Tropospheric Research, Leipzig; Harvard University; MIT; University of Windsor; Arizona State University; University of Wales, Cardiff; Ohio State University, etc. (Houghton, 1931; Houghton and Radford, 1938; Ruden *et al*., 1977; PWRI, 1988; Amanna, 1999; Colomb *et al*., 1999; Fortner, 1999; Saathoff *et al*., 2003; Colomb *et al*.,

* Corresponding authors.
E-mail address: tarun@iitk.ac.in; snt@iitk.ac.in

2004; Colomb *et al*., 2008).

The Fog Research Laboratory (FRL) was developed at Indian Institute of Technology Kanpur, India to conduct fog experiments. FRL consists of an in-house developed table top fog chamber facility which is designed to control most of the factors responsible for fog formation as in outside weather conditions. Experiments can be carried out using different FCNs at different condensing temperatures for different relative humidity and moist air flow rates.

The Fog Chamber Facility is unique of its kind in India and is made up of various components (Fig. 1), namely, a fog chamber, two types of aerosol generators, viz. dry and wet aerosol generators, Scanning Mobility Particle Sizer (SMPS, TSI Inc.), Cloud Combination Probe (CCP, DMT Inc.), two ultra-cold re-circulating cryostat chilled water circulators (chillers), hygrometer, steam generator and optical sensors. Several similar facilities around the world, that simulate artificial fog, are somewhat influenced by outside weather conditions, unlike that of ours.

Fog Research Laboratory (FRL)

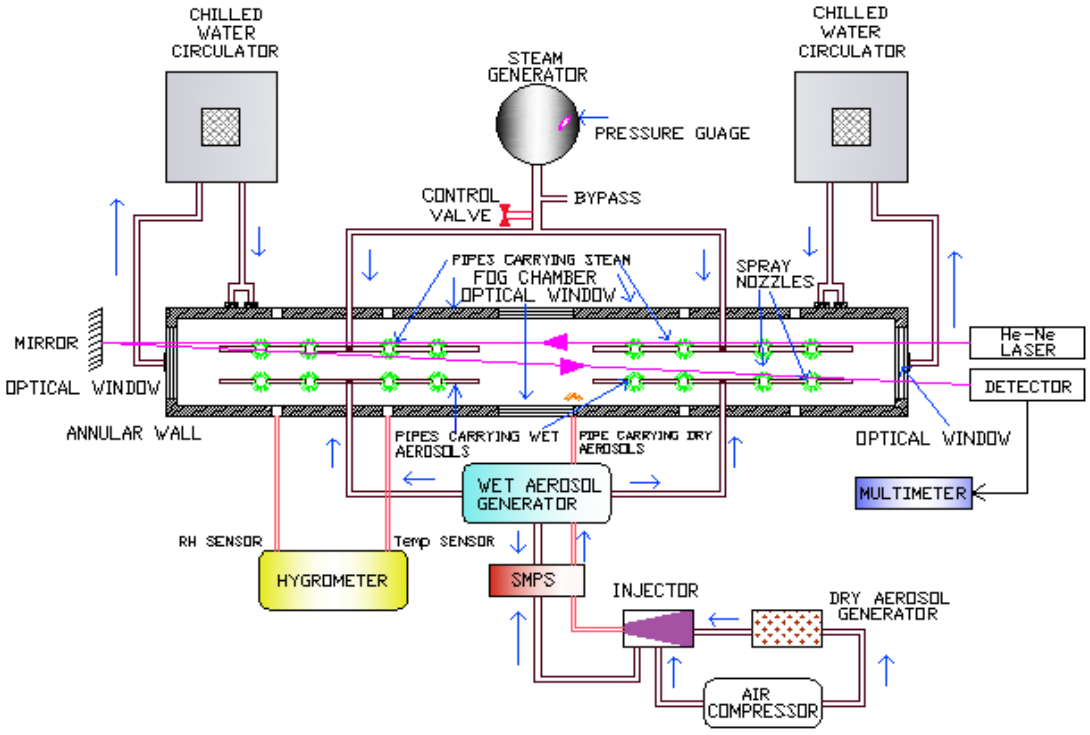

Fig. 1. Schematic and picture of Fog Chamber Facility with its Various Components: {(1)Fog Chamber, (2) Quartz window, (3) Needle valves, (4)Pipes for steam, (5) Pump, (6) Silica-gel dryer, (7) HEPA Filter, (8) SMPS probe, (9) He-Ne laser, (10) Detector, (11) Multi-meter, (12) CCP, (13) RH sensor, (14) Temperature sensor}.

Fog Chamber: It has an annular double walled, stainless steel, tunnel shaped box with a semi-circular cross section on the top and a rectangular cross-section at the bottom. The inner volume of the chamber is 0.8 m^3. There are four optical windows in the chamber for making optical observations and measurements.

Aerosol Generators: A portable atomizer (TSI Model 3079) was used for producing wet aerosol particles. The air flow rate was varied (50, 100 and 150 L/hr) by adjusting a valve. This controlled the total number of FCN entering the chamber. This atomizer can produce aerosol with constant size distribution and concentration with a high level of reproducibility. Another dry aerosol generator was developed in-house of brass and stainless steel for the dry aerosol generation as shown in the Fig. 2. Compressed air required for dispersing the aerosols in the generator was provided. A preset flow valve was used to set the air flow rate and the dry aerosol particle concentration was varied by simply adjusting the flow valve. Compressed air was supplied simultaneously to both the venturimeter inside the injector (Fig. 2) and dry aerosol chamber to produce aerosol with a stable size distribution.

Chilled Liquid Circulator: Raagaa's two chillers (using isopropyl alcohol) were used to create low temperatures inside the chamber to help fog formation. The tank capacity and size of each chiller were 50 L and 460 × 405 × 300 mm, respectively.

Humidity and Temperature Sensor: Humidity and temperature transmitter (HMT, Vaisala model 337) - a small device was employed to measure the temperature, T, Relative Humidity, RH, and dew point, inside the chamber with excellent accuracy and stability. It has RH measurement range of 0–100% with an accuracy of ± 1% at 20°C for 0–90% RH and ± 1.7% for 90–100% RH. It has temperature measurement range from –80°C to 180°C with an accuracy of ± 0.2°C at 20°C.

Steam Generator: Steam generator was a heat exchanger used to convert water into steam under high pressure and high temperature (100°C) by using a pressurised cooker of 20 L capacity. The moisture laden air was introduced inside the fog chamber and the moisture inside the chamber was controlled by adjusting the control valve.

He-Ne Monochromatic Laser: The linearly polarized He-Ne monochromatic laser beam (Uniphase, Model 102-4 (R)) was used for visibility measurements. The laser source produced monochromatic light at wavelength, λ, of 632.8 nm. The power of the source was 2 mW and the diameter of the beam cross section was approximately 0.73 mm.

Photoconductive Detector: The photoconductive detector was a silicon PIN photodiode -020A, having active area of 0.20 cm^2, used in the photoconductive mode where spectral range was from 350 to 1100 nm. The laser beam, which enters the chamber through a small optical window, is reflected by a plane silver mirror (99% reflectance at 633 nm), which had a flat surface placed on the opposite sides of the fog chamber (Fig. 1). The outer walls of the fog chamber were coated with black material to minimize losses.

Scanning Mobility Particle Sizer (SMPS): Measurement of particle (FCN) size distribution was carried out using Scanning Mobility Particle Sizer (SMPS, TSI Model 3936). The instrument was operated with a sheath flow rate of 3.0 L/min and an aerosol flow rate of 0.3 L/min.

Cloud Combination Probe (CCP): Measurement of fog droplet size distribution from 3 μm to 50 μm was carried out with Cloud Combination Probe (CCP) of Droplet Measurement Technology (DMT)**.** It had a combination of many probes which were Cloud Droplet Probe (CDP), Cloud Imaging Probe (CIP) and Liquid Water Content Sensor (LWC). CDP was particularly used for the measurement of cloud droplet size distribution. Since, fog droplets produced inside chamber have significantly high concentration therefore a special aspirator was used to aspirate fog droplet samples before they were detected by CDP. More details about Cloud Droplet Probe and its performance can be found elsewhere (Baumgardner *et al*., 1992; Baumgardner *et al*., 2001).

Theoretical Calculations

This section presents some basic calculations carried out to get an idea about the fog droplet growth and dissipation rates inside the newly designed fog chamber. Several

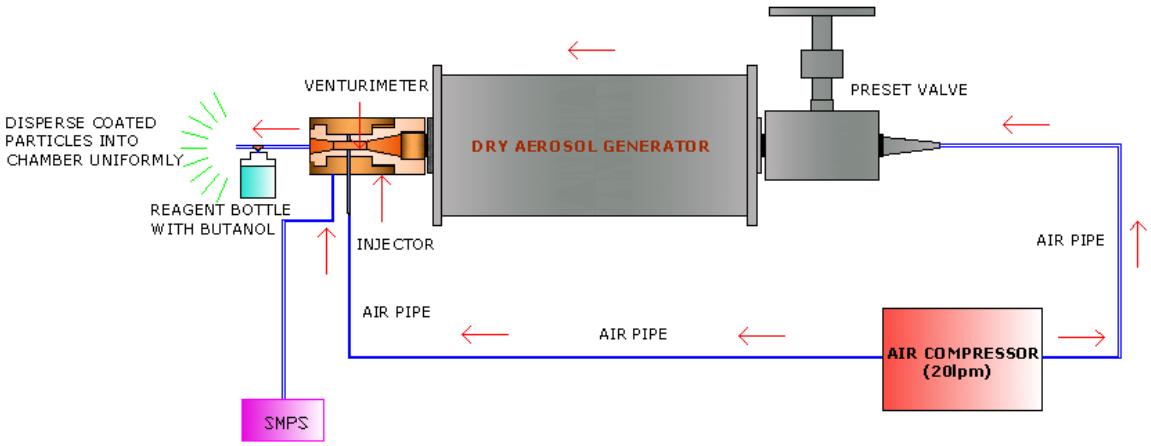

Fig. 2. Schematic of Dry Aerosol Generator showing the arrangement for making coated particles.

researchers in the past have attempted to accurately calculate the droplet growth and evaporation rates with different fluids including water (Hinds, 1999; Demokritou *et al*., 2002; Chate and Devara, 2005; Seinfeld and Pandis, 2006; Varghese and Gangamma, 2007). In addition, droplet effective radii were calculated using a set of well known equations (Hansen and Travis, 1974).

(A) Effective Radius

The scattering and extinction coefficients, K_{sca} and K_{ext}, respectively, are given as

$$K_{sca} = \int_{r_1}^{r_2} \sigma_{sca}(r) n(r) dr = \int_{r_1}^{r_2} \pi r^2 Q_{sca} n(r) dr \quad (1)$$

$$K_{ext} = \int_{r_1}^{r_2} \sigma_{ext}(r) n(r) dr = \int_{r_1}^{r_2} \pi r^2 Q_{ext} n(r) dr \quad (2)$$

where, n(r) dr is the number of particles per unit volume of air with radius between r and dr, σ_{sca} and σ_{ext} are the scattering and extinction cross section area, Q_{sca} and Q_{ext} are the efficiency factors for scattering and extinction, and r_1 and r_2 are radii of the smallest and largest particles in the size distribution.

The amount of light scattered by each particle is $\sigma_{sca} = \pi r^2 Q_{sca}$, so the best single parameter that describes the scattering is the mean radius for scattering (Hansen and Tarvies, 1974)

$$r_{sca} = \frac{\int_{r_1}^{r_2} r \pi r^2 Q_{sca} n(r) dr}{\int_{r_1}^{r_2} \pi r^2 Q_{sca} n(r) dr} \quad (3)$$

Similarly,

$$r_{ext} = \frac{\int_{r_1}^{r_2} r \pi r^2 Q_{ext} n(r) dr}{\int_{r_1}^{r_2} \pi r^2 Q_{ext} n(r) dr} \quad (4)$$

The appearance of Q_{ext} in Eq. (4) makes it an inconvenient parameter. However, if the wavelength of light is smaller then r_{ext}, a parameter can be obtained by omitting Q_{ext} which gives results as good as by Eq. (4). Thus, the R_{eff} is defined as,

$$r_{eff} = \frac{\int_{r_1}^{r_2} r \pi r^2 n(r) dr}{\int_{r_1}^{r_2} \pi r^2 n(r) dr} = \frac{1}{G} \int_{r_1}^{r_2} r \pi r^2 n(r) dr \quad (5)$$

where, G is the geometrical cross section area of the particles per unit volume.

(B) Droplet Growth in the Fog Chamber

Particles can follow two growth paths depending on their original size: (1) particle diameter, *D,* is less than gas mean free path, and (2) particle diameter is greater than gas mean free path.

(1) Droplet Growth from 40 nm to 70 nm:

The rate of droplet growth in this size regime can be obtained from the following formula,

$$\frac{dD}{dt} = \frac{2M\alpha_c (P_\infty - P_d)}{\rho_p N_a \sqrt{2\pi mkT}} \quad (6)$$

where, M = molecular weight of the liquid, ρ_p = density of the liquid, N_a = Avogadro's number, P_∞ = ambient partial pressure of vapour, P_d = partial pressure at droplet surface, α_c = condensation co-efficient, m = mass of a vapor molecule, k = Boltzmann's constant, T = temperature. Let, for the experiments in FRL the droplet temperature is 3.5°C and the temperature of steam is 27°C which is coming out from the pipe. To find out partial pressure at droplet surface, saturation vapor pressure which is responsible for forming the droplet (i.e. at temperature of 3.5°C) and Kelvin ratio are calculated (Hinds, 1999).

An empirical expression for the saturation vapor pressure of water is

$$P_s = EXP\left(16.7 - \frac{4060}{T - 37}\right) \quad (7)$$

where, T is the temperature in K.

The Kelvin Ratio, K_R, given as,

$$K_R = \frac{P_d}{P_s} \quad (8)$$

where, P_d is the partial pressure at droplet surface.

Also,

$$K_R = \exp\left[\frac{4\gamma M}{\rho RTd^*}\right] \quad (9)$$

where γ, M, and ρ are, respectively, the surface tension, molecular weight, and density of the droplet liquid. d^* is the Kelvin diameter. The values of $\gamma = 0.07512$ kg·m^2/s^2, M = 18 g/mol, ρ= 1000 kg/m^3, R = 8.31 m^3·Pa/K·mol, T = 276.5°K, d^* = 40 nm are used.

From Eq. (9), the value of Kelvin ratio and the value of saturation vapor pressure can be obtained from Eq. (7). By substituting these values in Eq. (8), one can get the value of partial pressure at droplet surface (P_d). The relative humidity, RH, of steam which is entering into the chamber is defined as,

$$RH = P_\infty/P_s \quad (10)$$

where, P_s is the saturation vapor pressure at the temperature of steam (in this case, 27°C), and P_∞ is the partial pressure of steam. Using the value of RH, and P_s from steam tables, the value of P_∞ the partial pressure of vapour can be obtained. Substituting all these values in Eq. (6), the time required for the droplet growth is obtained. For 3.5°C temperature, value of saturation vapor pressure (P_s) from Eq. (7) is 777 Pa. Substituting these values in Eq. (9) one gets K_R = 1.06. From Eq. (8), value of partial pressure at droplet surface is obtained as,

P_d = 824 Pa

RH of the moist air (steam) which is entering into the chamber for a typical experiment is 30% and the value of saturation vapor pressure of steam at 27°C is 3.57 kPa.

Substituting these values in Eq. (10), the value of partial vapor pressure is,

P_∞ = 1071 Pa

Using M = 18 g/mol, α_c = 0.04, P_∞ = 1071 Pa, P_d = 824 Pa, ρ_p = 1000 kg/m^3, $N_a = 6.023 \times 10^{23}$ 1/mol, $m = 2.98 \times 10^{-26}$ kg, $k = 1.38 \times 10^{-23}$ kg·m^2/s^2, T = 276.5°K, and solving Eq. (6) for time one gets 1.3×10^{-3} s for a droplet of initial diameter of 40 nm to grow to a final diameter of 70 nm .

(2) Droplet growth from 70 nm to 16 μm:

Once particle has grown upto the gas mean free path, growth depends, not on the rate of random molecular collisions, but on the rate of diffusion of molecules to the droplet surface. In such case, the rate of droplet growth can be obtained from the following equation,

$$\frac{dD}{dt} = \frac{4D_V M}{R\rho_p D}\left(\frac{P_\infty}{T_\infty} - \frac{P_d}{T_d}\right)\Phi \quad (11)$$

where, D_V is the diffusion coefficient of water vapor and Φ is the Fuchs correction factor. The value of Fuchs correction factor can be obtained from following equation.

$$\Phi = \frac{2\lambda + D}{D + 5.33\left(\frac{\lambda^2}{D}\right) + 3.42\lambda} \quad (12)$$

where, λ is gas mean free path (~66 nm).

By substituting these values in Eq. (11), one can get the time required for the droplet growth, which is 2.72 s. Also, here Saturation Ratio, S_R = 1.3is used.

(C) Resident Time of Droplets in Fog Chamber

Moist air in the form of steam provides vapour for the particle growth present in the chamber. These particles grow and become droplets of different sizes. CDP measures the concentration of droplets from 3 to 50 μm. From the height of the chamber and settling velocity of droplets, resident time can be calculated. The value of slip correction factor (C_c) is important when diameter of particle (droplet) is less than 1 μm, which is ignored in this case as droplet size varies from 3 to 50 μm. Using the procedure laid out in Seinfeld and Pandis (2006, pp 411), one can get the value of settling velocity of particle (droplet).

$$C_D R_e^2 = \frac{4 \cdot \rho_p \cdot \rho \cdot g \cdot C_c \cdot D^3}{3\mu^2} \quad (13)$$

where, C_D = Drag coefficient, R_e = Reynold's number, ρ = Density of air, ρ_p = Density of droplet, g = acceleration due to gravity, C_c = slip correction factor, D = Diameter of droplet, μ = Dynamic viscosity.

By substituting the values of all the terms of right hand side of above equation, we get the value of $C_D R_e^2$.

For $R_e \leq 0.1$, the terminal settling velocity can directly be calculated by following formula given by Stokes law (Hinds, 1999),

$$v_t = \frac{\rho_p \cdot g \cdot D^2}{18\mu} \quad (14)$$

If $R_e > 0.1$, the terminal settling velocity can be calculated using following formula,

$$v_t = \frac{\mu \cdot R_e}{\rho \cdot D} \quad (15)$$

The ratio of height of chamber to the terminal settling velocity gives the total resident time of droplets in the chamber.

EXPERIMENTAL METHOD

Fog formation in the atmosphere is directly related to radiative, thermodynamical, aerosol and microphysical processes (Pruppacher and Klett, 1997). A large number of experiments were carried out in FRL in order to identify the combination of ambient conditions and characteristics of FCN in the atmosphere responsible for dense fog formation. Experiments were carried out to measure the rate of formation and dissipation of fog and droplet size distribution to understand the microphysics of fog using different types of FCN such as $(NH_4)_2SO_4$, NaCl, ambient air, uncoated and coated graphite for three different range of temperatures.

Fog Generation

Chamber was cooled by a closed loop circulation of Isopropyl alcohol from the chiller to flow through the annular walls of the chamber to maintain the desired temperature. As the desired fog chamber's temperature reached, steam and FCN with known properties were introduced simultaneously in the fog chamber through the showers located on the top. Two outlets provided at the

bottom of the chamber were opened to maintain atmospheric pressure inside the chamber. Once the steady state was achieved, moist air was brought under high pressure from spray nozzles as they enter into the chamber through two adjacent pipes.

Aerosols were injected inside the fog chamber using either wet or dry aerosol generators. A wet aerosol generator was used for dispersing wet aerosols through the nozzles attached to parallel tubes placed on the upper end of the chamber. Dry aerosol generator was used for dispersing dry aerosols into the chamber with high velocity with an injector nozzle connected to one side of the upper annular wall of the chamber to carry and disperse the aerosols uniformly.

Visibility Measurements

The generated fog is qualified by its visibility. The whole fog chamber assembly was kept in a closed room and all the experiments were performed in complete darkness. The optical visibility measurement was done using a He-Ne laser and a Si-detector along with a silver coated mirror. The laser and the detector were kept optically isolated at one end-on window of the fog chamber. The laser output was coupled to the detector, after a round trip passage through the chamber, with the help of the mirror placed on the opposite end window of the fog chamber, 2 m away. The measurement of fog visibility (V) in the units of meter was obtained from the transmission loss, T (λ = 633 nm) of the He-Ne laser through the Fog Chamber. A data logger was connected to the Si-detector to continuously monitor the visibility. The formulation for V was adopted from the definition of Meteorological Optical Range (http://www.wmo.ch/pages/prog/www/IMOP/publications/CIMO-Guide/Draft%207th%20edition/Part1-Ch09Final_Corr.pdf) as:

$$V = \frac{L \times \ln(0.05)}{\ln(T(\lambda))} \tag{16}$$

where L is the round trip length of the fog chamber and

$$T(\lambda, L) = \frac{P(\lambda, L)}{P(\lambda, 0)} = e^{-\sigma(\lambda)L} \tag{17}$$

where σ (λ) is the fog attenuation coefficient and

$$\sigma(\lambda) = \alpha(\lambda) + \beta(\lambda) \tag{18}$$

α and β being the absorption and scattering coefficient, respectively (Nebuloni, 2005).

It has been shown that the visibility changes in the same ratio as any wavelength in the human vision spectrum (http://neuronresearch.net/vision/files/photopiceffic.htm), hence measurement was only performed at λ = 633 nm. The roundtrip attenuation was normalized with respect to the "no-fog" condition, which eliminated errors due to all spurious reflection and scattering. The fog was assumed to be stable when there was no significant change in measured RH i.e. within ± 0.5% with an error in measuring "P" of 7.5% under the densest fog obtained. It is important to note that the change was not abrupt, as it happens when density of fog changes very rapidly. Moreover, all these experiments were carried out under atmospheric pressure and the effects of radiation was not accounted for.

Measured Aerosol Distribution

Two sets of experiments (A) and (B) were performed in the FRL. In (A), parametric investigations were carried out in terms of change in FCN concentration, chemistry of FCN, and different supersaturation conditions kept inside the FRL. Whereas in (B), effect of mixing of FCN having different chemical composition with ambient air on the fog formation was studied.

(A) Fog inside the chamber was created using different FCN and their dissipation rates were compared at different flow rates and for different temperature ranges. For a particular range of temperature (3.5 ± 0.2°C, 4.5 ± 0.2°C and 5.5 ± 0.2°C) experiments were performed at different flow rates of 50 and 100 L/hr for wet aerosols and 18 L/hr for dry aerosols, respectively. Wet aerosol generator was used to distribute $(NH_4)_2SO_4$ and dry aerosol generator was used to inject uncoated and coated graphite particle inside the chamber. The arrangement for making coated graphite particles and injecting it into the chamber is shown in Fig. 2. An arrangement was made to fit a bottle containing fixed amount of organic solvent (Butanol, Reagent Grade, Merck) in front of dry aerosol generator at room temperature. Uncoated particles from the dry aerosol generator were passed through the dense vapour of volatile organic material whose saturation temperature was much lower compared even to the room temperature (~30–32°C).

(B) Different fog condensation nuclei (FCNs) such as sodium chloride (NaCl), uncoated graphite, their mixture with ambient air etc. were used to generate fog. A HEPA filter was used at the inlet of the chamber to almost completely remove the particles present inside the FRL (evacuated case). Once the particle concentration of less than 50 #/cm^3 was obtained, the clean air flow was stopped by needle valve provided at T joint. After this, steam was passed to get moist air for the fog formation. Steam was passed for about 5 min and then FCN were introduced into the fog chamber by opening the needle valve at T joint. Optical measurements were carried out to determine stable fog. Time was recorded when the voltmeter showed a constant value. Once the stable fog was obtained, fog droplet size distribution was measured using Cloud Droplet Probe (CDP). During all these steps, temperature of the chamber was kept constant. The following six different FCN cases were considered: evacuated chamber, ambient air, mixed (ambient + NaCl) particles, mixed (ambient + graphite) particles, only NaCl particles, and only graphite particles, respectively.

RESULTS AND DISCUSSION

The results of fog formation, persistence and dissipation are presented and discussed in three parts; the first one (A) describes the relationship between microphysics of fog and

visibility, and (B) discusses the effect of varying FCN chemical properties on the degree of fog stability. In addition, the effect of temperature on the dissipation rate of artificial fog formed by individual species is discussed and compared with theoretically calculated values. The analysis of total extinction by effective radius method is presented in the final section.

Relationship between Microphysics of Fog and Visibility

(A) Particle size distribution for $(NH_4)_2SO_4$ (ammonium sulphate), coated and uncoated graphite measured with SMPS at different flow rates is shown in Figs. 3(a) and (b). It can be seen that the particle size distribution for $(NH_4)_2SO_4$ is wider for small particles. Most of the particle lies in the ultrafine range and the mode for the distribution is less than 40 nm. On the other hand, uncoated and coated graphite particles show bimodal distribution with 30 and 200 nm modes, respectively. The number of particles entering in the chamber in one minute was quite comparable among all the four configurations as depicted in Table 1.

A number of experiments using different FCNs were carried out for visibilities ranging from 3 to 125 m for three temperature ranges viz. 3.5 ± 0.2°C, 4.5 ± 0.2°C and 5.5 ± 0.2°C, corresponding to three different supersaturation conditions inside the chamber, respectively. Five visibilities viz. 3 m, 10 m, 20 m, 50 m and 125 m have been chosen for which droplet distributions are shown. Visibilities in fog were calculated using equations as described before. Simultaneous measurements of droplet distribution and visibility were made to know exactly the characteristics of droplet size distribution at a particular visibility.

Figs. 4(a), (b) and (c), for $(NH_4)_2SO_4$ show that the temperature has clear effect on the droplet number concentration. At 3.5°C the droplet number concentration is slightly higher at any given visibility compared to those at 4.5°C and 5.5°C, respectively. In particular, droplet concentrations at the small drop size end increases as the temperature reduces (at 5.5°C the concentration of 3 µm diameter particles is about 105 number droplets 1/cm^3 that rises to 220 number droplets 1/cm^3 at 3.5°C at 3 m visibility, Figs. 4(a), (b)). However, the overall number of fog droplets formed for 50 L/hr and 100 L/hr cases are more or less similar.

These results show some kind of trend for dense fog conditions whereas at higher visibility levels entirely different behaviour was observed. At higher visibility levels some droplets size distributions (DSD) are crossing

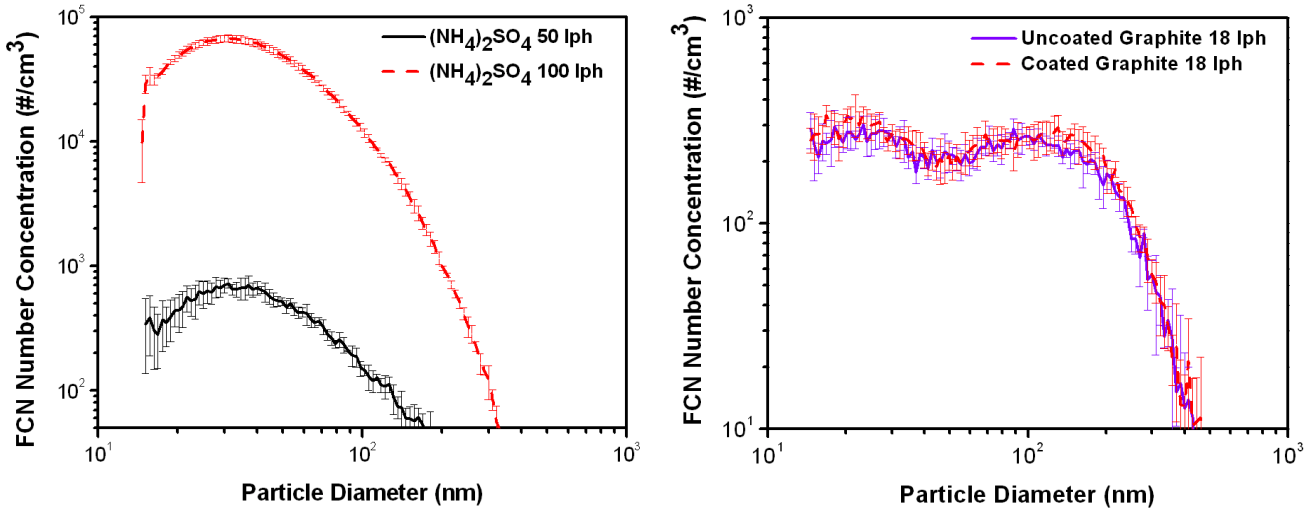

Fig. 3. (a) Average FCN size distributions for Ammonium Sulphate particles at 50 and 100 L/hr flow rate produced by the wet aerosol generator from 0.05 g/lit Ammonium Sulphate solution measured with SMPS. (b) Average FCN size distributions for coated and uncoated graphite particle at 18 L/hr flow rate produced by the dry aerosol generator measured by SMPS. Scan time 3 minutes each for 5 samples.

Table 1. Number of FCN particles entering into the fog chamber.

FCN	Flow rate (L/hr)	Number of FCN particles entering into fog chamber[a] (#/min)	GSD
Ammonium Sulphate	50	2.24×10^7	1.7
Ammonium Sulphate	100	4.20×10^7	1.6
Uncoated Graphite	18	3.78×10^7	2.3
Coated Graphite	18	4.10×10^7	2.3

[a] The number of particles entering into the fog chamber in one minute time interval for each experiment was determined by multiplying average concentration (particles/cm^3) with flow rate and time. Average size distribution of FCN particles at set flow rates and measured by SMPS, were used to compute aerosol number concentration.

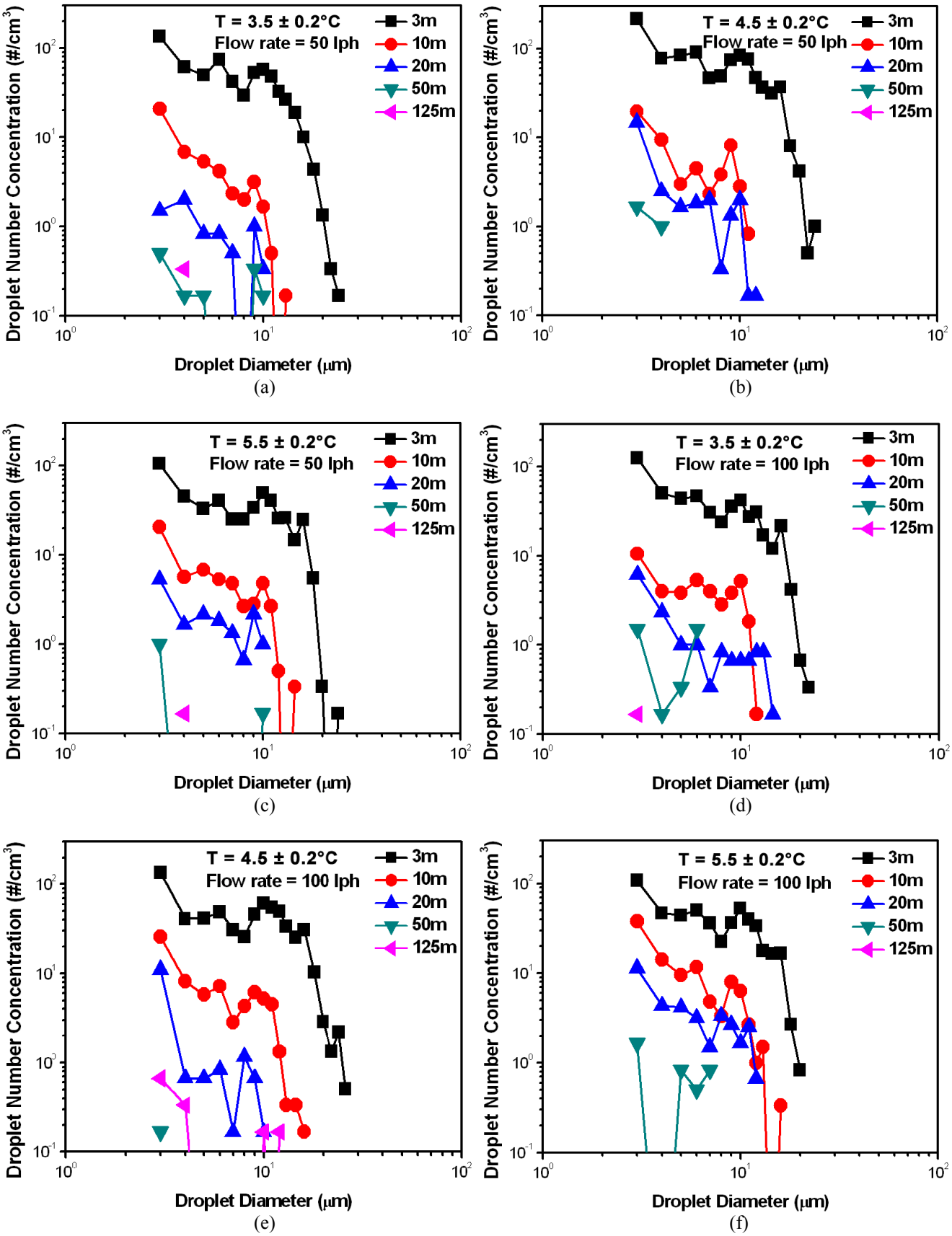

Fig. 4. (a), (b) and (c) Fog droplet size distribution at temperatures 3.5 ± 0.20°C, 4.5 ± 0.20°C and 5.5 ± 0.20°C, respectively, when $(NH_4)_2SO_4$ is used as FCN for various visibility conditions for 50 L/hr flow rate. Figs (d), (e) and (f) show same results except for 100 L/hr flow rate.

each other, this might be owing to the fact that for these DSD the range of number concentration for all size bins was between 0–10 number droplets 1/cm^3 but the R_{eff} for all these visibilities are different which will be discussed in next section. Clearer droplet size distribution at higher visibilities has been seen in case of $(NH_4)_2SO_4$ in which wide DSD was observed at different higher visibility level. The results for $(NH_4)_2SO_4$ from Figs. 4(a), (d) also show that with the increase of flow rate, at a particular temperature and for low visibility levels, the size distribution gets marginally broader (GSD is 1.8 for 3.5°C at 50 L/hr flow rate and 1.9 for 3.5°C at 100 L/hr flow rate).

A very interesting result has been seen in case of uncoated graphite Figs. 5(a), (b) and (c) that even at higher visibilities the number concentration of droplets was much higher compared to hygroscopic particles of $(NH_4)_2SO_4$ and, secondly, a wide DSD is obtained at higher visibilities that was not the case in $(NH_4)_2SO_4$. This is likely due to presence of abundant smaller droplets of $(NH_4)_2SO_4$ (< 3 μm) that could not be actually measured by CDP under higher visibility conditions. The CDP has a lower size detection limit of 3 μm. Whereas, SMPS had an upper size detection limit of 0.8 μm. Simultaneous measurements were made to measure DSD and visibilities and it may happen that a fraction of attenuation was caused due to these small droplets (< 3 μm) in case of $(NH_4)_2SO_4$ due to which variation was observed in the DSD's of hygroscopic compound and coated graphite. The droplet size distribution ranged from 3 μm size droplet to 24 μm. In very dense fog conditions (i.e. visibility = 3 m) the biggest droplet observed were 23 μm for $(NH_4)_2SO_4$, 24 μm for uncoated graphite particles and 22 μm for coated graphite particles. The CDP probe was kept almost at the centre of the fog chamber to measure the fog DSDs. It is worth pointing out that DSD values reported throughout this paper corresponds to only stable fog conditions and no transient values (during growth and dissipation of fog droplets) are provided.

It was found that for all tested FCNs and temperatures as the fog dissipates, almost same trend in the DSD was seen with a shift in droplet to lower size and number concentration. Differences in droplet distributions compared to coated graphite were observed but the distribution was highly uneven. The number concentration at higher temperature was very less and DSD got broader in case of uncoated graphite (GSD for uncoated graphite at 3.5, 4.5 and 5.5°C were 1.6. 1.6 and 1.8, respectively, while GSD for coated graphite at 3.5, 4.5 and 5.5°C were 1.4, 1.4 and 1.8, respectively). Even at higher visibilities there were lots of droplets and almost all droplet sizes were present even for visibility = 15 m.

This is an interesting observation as no distinct differences were observed between fog generated using coated Vs uncoated graphite for all three different Supersaturation conditions tested. For instance, the 3.5°C condition corresponds to a Supersaturation of 1.3. This indicates to the fact that at such high supersaturation conditions droplet activation was nearly uniform and there was hardly any effect of hygroscopicity of the FCN on its activation and growth rate for dense fog conditions (Gupta *et al*., 2004). It is important to note here that natural ambient conditions under which fog formation takes place are always at marginal supersaturation conditions (~1.05) (Bott, 1991).

(B) Fig. 6(a) shows the particle size distribution for different FCN tested to generate fog for this set of experiments. Fig. 6(b) shows the fog droplet size distribution for these different cases. Table 2 provides the average (n = 5) droplet number concentration in the fog chamber for these different cases studied. The effects of different fog condensation nuclei chemical composition and number concentration are clearly visible on fog droplet size distribution. The droplet number concentration was quite high in NaCl-only case than mixed (ambient + NaCl) case. There was not only higher droplet concentration in NaCl-only case compared to other cases, but there was also change in pattern of fog droplet size distribution with a shift in peak (Fig. 6(b)). Peak concentration for NaCl-only case was at 16 μm, while it was at 6 μm for rest of the cases (Table 2). This suggests abundance of bigger size droplets for the NaCl-only case.

Droplet growth calculation using published literature showed that a particle of 70 nm takes about 2.72 s to become a droplet of 16 μm at a supersaturation (Sr) = 1.3. However, in our experiments the time taken to get stable fog using optical measurements were 7 min, 9 min and 10 min with NaCl only, ambient and mixed (ambient + NaCl) cases, respectively. The experimentally observed times to generate stable fog are much longer suggesting some missing links here. One possibility could be that at an Sr = 1.3, all FCN get activated almost instantaneously and there is a lack of sufficient water vapour to carry out further droplet growth resulting in slower droplet growth. Although, this needs to be verified in the lab as in the current study droplet growth kinetics were not studied.

Any form of inhomogeneity in terms of Sr (i.e. T and water vapour concentration) within the chamber may have also substantially delayed the formation of stable fog since we were measuring the level of stability of the fog using very fine electro-optical means (Zhang and Liu, 1990). This might be a significant reason since with naked eye (via Quartz windows) we could see fog formation taking place almost instantaneously in the fog chamber but the voltmeter showed fluctuations for a long time. These points towards internal adjustments occurring within the generated fog leading to longer times in producing a stable voltmeter reading.

These results also suggest that in presence of ambient particles, NaCl FCN takes longer time to generate a stable fog layer. This may be because the ambient particles are somewhat inhibiting the complete growth of NaCl particles to become larger droplets (Hansson *et al*., 1998; Mickey *et al.*, 1990).

Effect of Temperature on Fog Dissipation Rate

(A) Dissipation of $(NH_4)_2SO_4$ fog as FCN and as a function of visibility for different flow rate of 50 and 100 L/hr are shown in Fig. 7. It can be seen that for different sets of experiments even a 1°C reduction in temperature

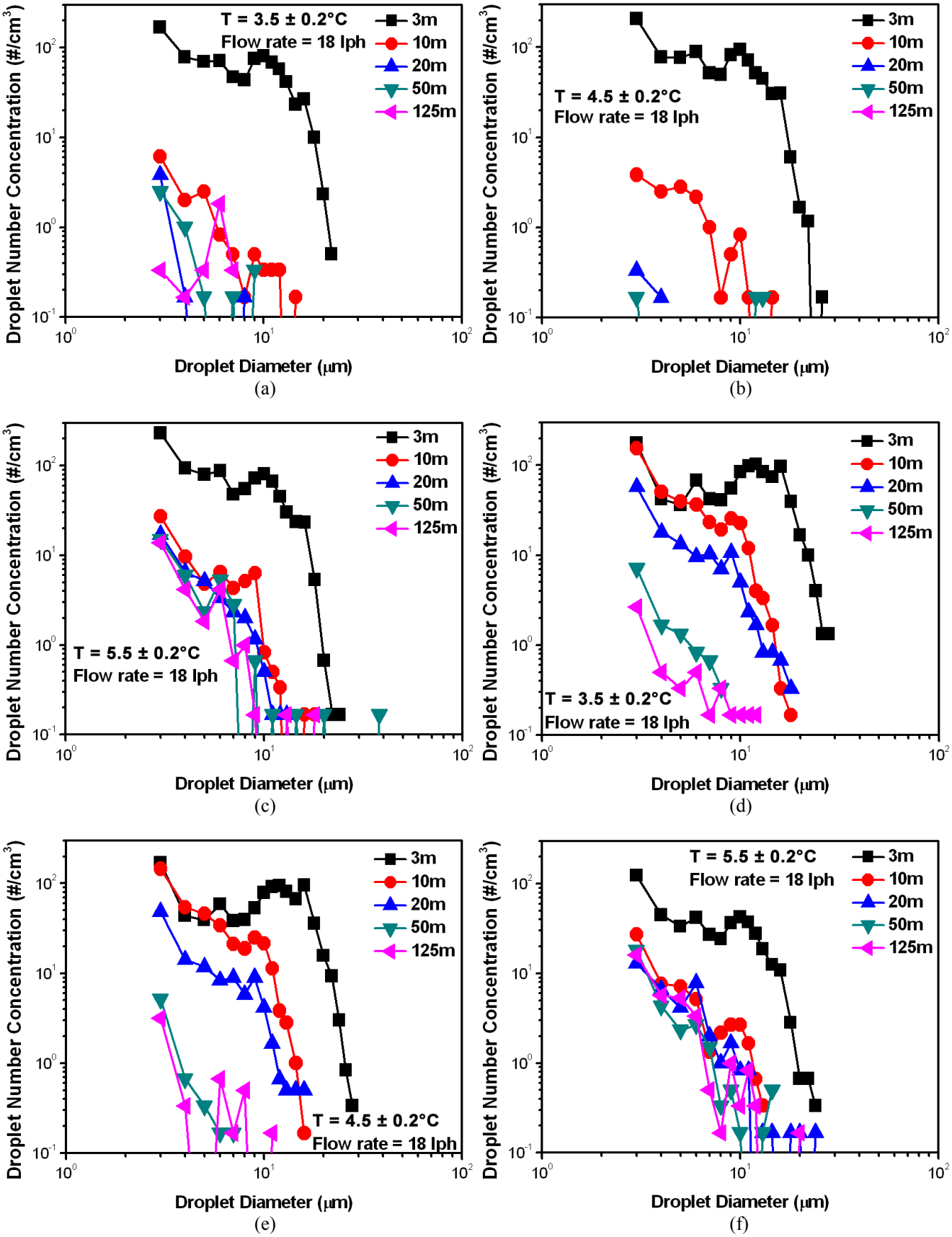

Fig. 5. (a), (b) and (c) Fog droplet size distribution at temperatures 3.5 ± 0.20°C, 4.5 ± 0.20°C and 5.5 ± 0.20°C, respectively, when uncoated graphite is used as FCN for various visibility conditions for 18 L/hr flow rate. Figs (d), (e) and (f) show similar results for coated graphite distribution at temperatures 3.5 ± 0.20°C, 4.5 ± 0.20°C and 5.5 ± 0.20°C for 18 L/hr flow rate.

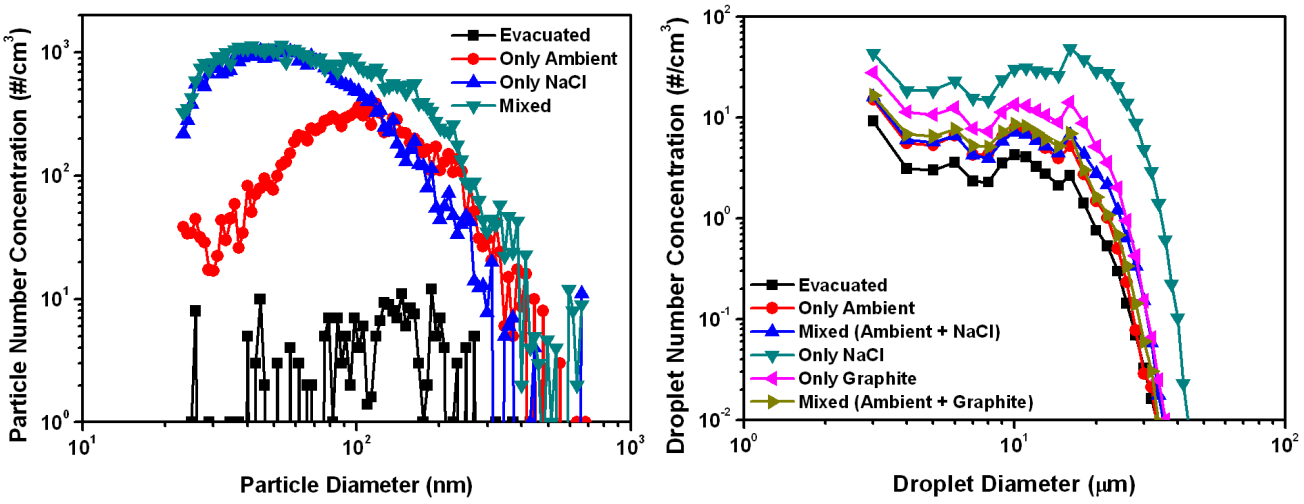

Fig. 6. (a) Particle size distribution for different cases, and (b) droplet size distribution for different cases.

Table 2. Average (n = 5) fog droplet number concentration in the fog chamber for different cases.

FCN Type	(#/cm^3)
Evacuated	49 ± 35
Ambient	89 ± 65
Only NaCl	500 ± 251
Mixed (Ambient + NaCl)	97 ± 61
Only Graphite	182 ± 106
Mixed (Ambient + Graphite)	104 ± 56

has a significant effect on fog dissipation. The dissipation of fog basically happens through coalescence of several smaller droplets into larger droplets and subsequent gravitational settling process, so Fig. 7 shows that the rate of coalescence decreases with decrease in temperature. It can be seen that for ammonium sulphate fog, for 50 L/hr and 100 L/hr, the fog dissipation rate (ΔVisibility/ΔTime) decreases with the decrease in temperature for the same environmental conditions i.e. FCN number concentration and pressure. This can be understood by analyzing the droplet distribution data for $(NH_4)_2SO_4$ shown in the previous section, for lower temperature inside the fog chamber (higher Sr) more number of smaller droplets were formed compared to that at higher temperature (lower Sr) that was responsible for lower dissipation rate as it takes more time by smaller droplets to coalesce to bigger droplets and get removed. For very dense fog conditions when the visibility level was less than 18 m, the fog dissipation rate was almost same for all FCNs at particular flow rate and different temperature ranges except for coated graphite case in which a deviation was observed at low visibilities.

It seems that at a temperature of 6.5°C (Sr marginally above unity) inside the fog chamber very few graphite particles got activated into fog droplets. Again coated graphite particles might have got activated little faster than uncoated graphite owing to lower Sr. So the results for 6.5°C in Fig. 8 shows unusual deviation from that seen for $(NH_4)_2SO_4$ in Fig. 7.

The rate of dissipation within this lower visibility region upto 18 m in Fig. 7 was almost same for all temperature range but it was observed that the rate decreases with increasing flow rate. The reason being droplet distribution of $(NH_4)_2SO_4$ for all temperature ranges and at low visibility gets broader with increasing flow rate and more number of small size end droplets were formed and basically they were responsible for the decreasing fog dissipation rate with increasing FCN flow rate.

Visibility through fog for uncoated and coated graphite as FCN and as a function of time for different flow rates are shown in Fig. 8. Highly uneven dissipation curves were obtained for uncoated graphite. These do not follow any particular pattern. In Fig. 8(a) for uncoated graphite, the dissipation curve for 3.5 and 4.5°C follow almost the same path and dissipation curve for 5.5 and 6.5°C upto 40 m but after that there was a variation in dissipation rate pattern. This is also visible from droplet distribution for uncoated graphite where no particular pattern in DSD has been observed. Measured visibility in coated graphite (Fig. 8 (b)) shows that the trend is similar to ammonium sulphate fog and the rate of fog dissipation decreases as the temperature decreases (increasing Sr) except at 6.5°C (Sr marginally above unity) which showed marked deviations from the common trend.

(B) Theoretical calculations using previously published set of equations suggests that it should take around 19 min for a 16 μm fog droplet to reach to bottom of the fog chamber (Fig. 9). The ratio of height of chamber to the terminal settling velocity gives the total resident time of droplets in the chamber. Fig. 9 shows the resident time of droplets from 3–50 μm. By this time other sets of particles which are entering into the chamber are continuously growing into similar sets of droplets, which are settling at the same rate and which would result in the stable fog. But the results from optical measurements showed that NaCl-only based fog took around 7 min to get stable. This may be because of the droplets of size more than 16 μm present in the chamber which would have settled faster and the

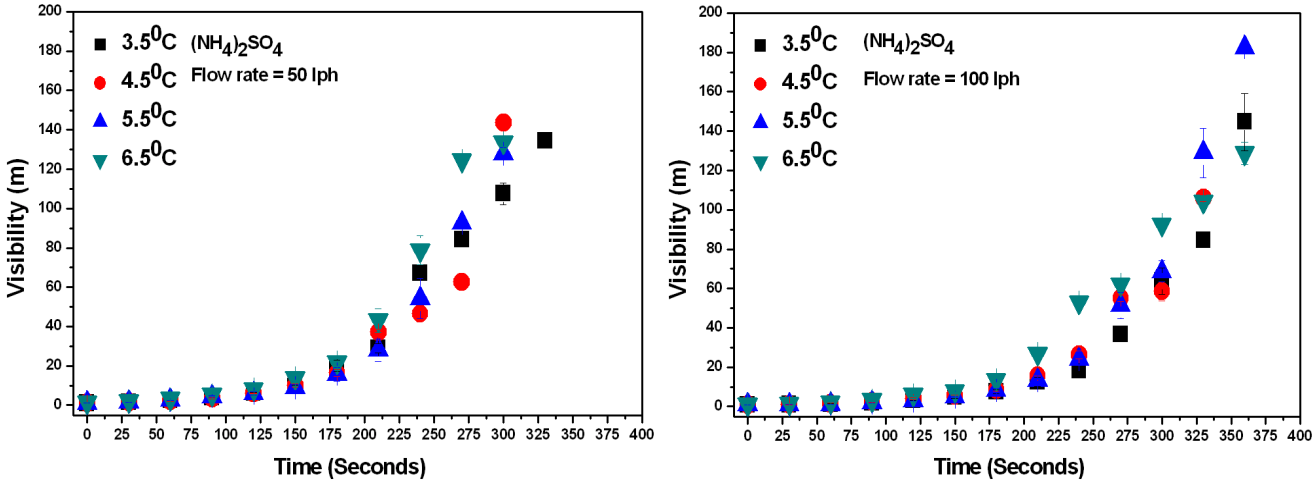

Fig. 7. Visibility of dissipating fog as a function of time for $(NH_4)_2SO_4$ (Ammonium Sulphate) acting as FCN for a flow rate of (a) 50 L/hr and (b) 100 L/hr.

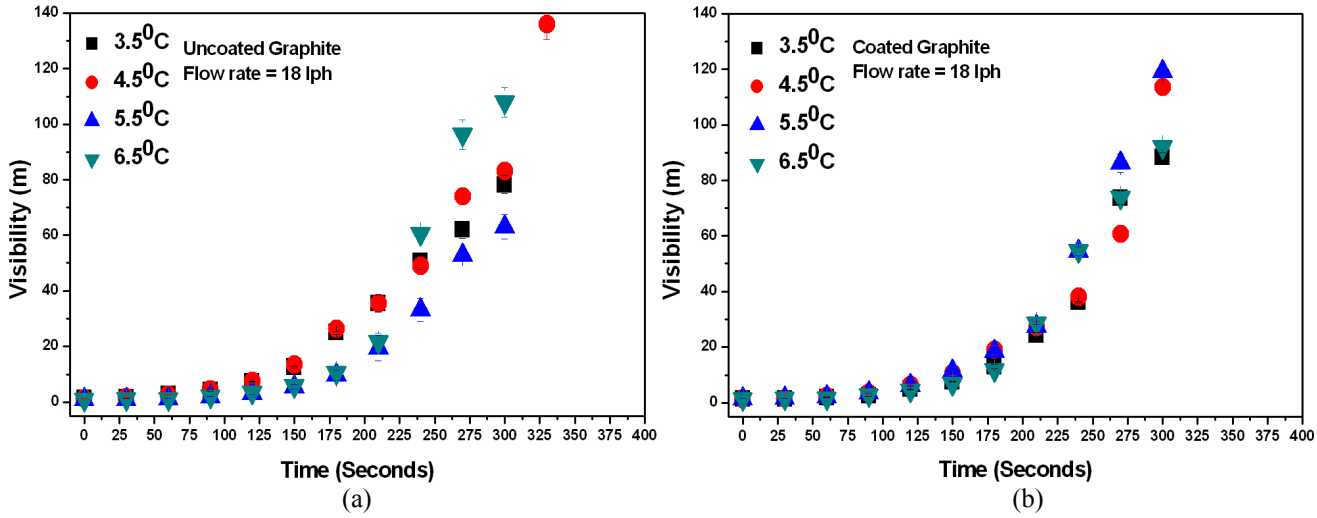

Fig. 8. (a) Visibility of dissipating fog as a function of time for a flow rate of 18 L/hr for (a) uncoated graphite acting as FCN and (b) coated graphite acting as FCN.

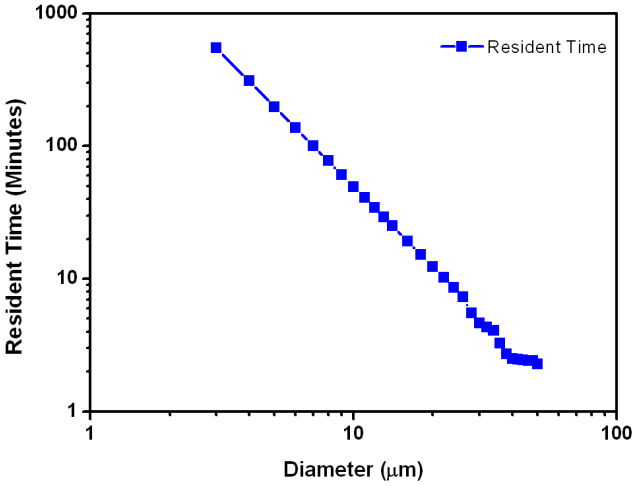

Fig. 9. Resident time of droplets in fog chamber for different sizes.

other reason may be the size of droplets which we have taken into consideration for calculation (16 μm) may not remain 16 μm till it settles to the base of the chamber because there may be a further droplet growth which may further increase the settling velocity. Please recall that the CDP was kept at the centre of the fog chamber and it is likely that it may have missed the bigger droplets which were still growing as they pass the mid-section of the chamber while settling down.

Also, separate experiments were conducted to know the dissipation rate of fog for different FCNs. Results of these experiments showed that fog of mixed (ambient + graphite) FCN particles persisted for maximum duration (7 min) after getting stabilized and fog of ambient particles persisted for minimum duration (4 min) after getting stabilized, while NaCl only based fog took about 5 min for dissipation after getting stabilized. This observation has huge implications in terms of higher ambient pollution (more carbonaceous soot)

and occurrence of stable fog episodes. Although, this requires much more detail investigations.

Analysis of Total Extinction Due to Droplet Size Distribution Using Effective Radius Method

(A) To extend the present work we focused on the analysis of total extinction due to droplet size distribution using R_{eff} method. This method of calculating the total extinction by droplet size distribution consists of finding an equivalent radius that has same optical properties as of total droplets in a droplet size distribution. Effective radius, R_{eff}, is defined as the equivalent radius of droplet that has optical properties (total extinction, scattering), similar to the optical properties of whole droplet size distribution. If the total extinction is same then the R_{eff} for these DSDs should be nearly same. This parameter was defined as the ratio between the third moment to the second moment of a droplet size distribution. The detail calculations for R_{eff} are provided in an earlier section.

R_{eff} calculated for different FCNs at particular visibility for different flow rates and temperatures are shown in Table 3 and 4. R_{eff} for five visibilities viz. 3 m, 10 m, 20 m, 50 m and 125 m were calculated. In order to verify the total attenuation by DSDs a computer program was used based on trapezoidal integration method that directly gave the R_{eff} for a particular DSD.

It has been shown in the previous section that for $(NH_4)_2SO_4$, temperature (or Sr) has an increasing effect on number concentration, more number of smaller size droplets were formed at lower temperature (higher Sr) and DSD gets broader with decreasing temperature (increasing Sr). Secondly, with the change in characteristics of FCN size distribution i.e. with increasing flow rate the resultant fog DSD also got broader. The same was happening with all FCNs except for uncoated graphite.

It was observed from R_{eff} data given in the Table 3 and 4, that although characteristics of DSD for different flow rates and temperature were different but the R_{eff} calculated was almost similar at a particular visibility which verifies our results that the total attenuation for a particular FCN for different flow rate and temperature (i.e. for a given Sr) was same.

For visibility less than 50 m, for all FCNs, the standard deviation in calculation of R_{eff} was small. The reason being, in fog DSDs at higher visibilities, the bigger size droplets more than 10 μm were rare, in other words droplets in higher size bins were absent in the droplet distribution due to which calculation from modelling deviates.

It has been observed from Table 4 that the standard deviation in calculation of R_{eff} was very less in case of coated graphite compared to $(NH_4)_2SO_4$. The reason being $(NH_4)_2SO_4$ is hygroscopic due to which there were probably more number of smaller droplets (< 3 μm) formed in the chamber, that could not be measured by CDP but these droplets were also responsible for the attenuation. Simultaneous measurements were made to measure DSDs of various FCNs and visibility through fog. Since we have taken the DSD at a particular visibility, it may happen that in the calculation of visibility there was some contribution of these small size droplets in attenuation, the number concentration of those was possibly different at different temperatures and flow rates for $(NH_4)_2SO_4$ and due to this small variation, the R_{eff} were little bit different.

CONCLUSIONS

This paper presented a state-of-the-art facility to generate fog under carefully controlled conditions. Different FCNs

Table 3. Effective radii of Ammonium Sulphate $(NH_4)_2SO_4$ for different flow rates and temperatures at particular visibilities.

Ammonium Sulphate								
Effective Radius (μm)								
Visibility in metres	3.5°C		4.5°C		5.5°C		Average	Std. deviation
	50 L/hr	100 L/hr	50 L/hr	100 L/hr	50 L/hr	100 L/hr		
3	6.833	6.142	6.31	6.822	6.283	5.938	6.388	0.365
10	3.69	4.201	3.951	4.549	4.272	4.361	4.17	0.306
20	3.647	5.126	3.865	3.383	3.809	4.246	4.013	0.614
50	4.245	2.763	1.840	1.5	4.255	2.985	2.931	1.162
125		3		3			3	0

Table 4. Effective radii of Uncoated and Coated Graphite for different flow rates and temperatures at particular visibilities.

Effective Radius (μm)										
Visibility in metres	Uncoated Graphite					Coated Graphite				
	3.5°C	4.5°C	5.5°C	Average	Std. deviation	3.5°C	4.5°C	5.5°C	Average	Std. deviation
3	6.148	6.077	5.818	6.014	0.173	7.635	7.543	5.990	7.0566	0.924
10	4.277	3.941	4.111	4.109	0.168	4.321	4.173	4.005	4.166	0.158
20	2.415	1.820	3.435	2.556	0.816	4.612	4.260	5.667	4.846	0.732
50	3.144	6.237	9.825	6.402	3.343	2.692	2.191	4.239	3.040	1.067
125	2.898		4.191	3.544	0.914	4.142	3.575	4.504	4.074	0.468

were used to generate fog and their effect on the formation, stability and dissipation of fog were studied. Parametric investigations were performed by varying supersaturation conditions inside the fog chamber.

A 70 nm FCN grew to 16 μm drop in just 2 min as determined from experimental observations using visibility reduction as proxy. Theoretically, it should get to that size even much faster (2.72 s) given the supersaturation conditions (S_r calculated to be 1.3) are homogenous and there are no other competing phenomena in place. Also, once the FCN grows into the fog droplet they are all the same no matter what the original chemical composition, morphology or size of the FCN was as now close to 99% of it is water. However, FCN like NaCl, $(NH_4)_2 SO_4$ would completely dissolve inside the droplets while soot (coated or uncoated) will still remain as a distinct nuclei inside the droplets. As large fraction of drop is water the nuclei will not affect the surface properties.

It is also observed that the fog dissipates faster, 4–7 min rather than 19 min time that is predicted by the simple gravitational settling calculations for the fog droplets (mode 16 μm). This suggests that some other mechanism maybe significant in removal of the fog. Other scenario could be that the fog droplets might be continuously growing even while settling down resulting in their faster removal rates. Sr clearly comes out as a critical parameter both from the fog dissipation rate results and calculated R_{eff} for different FCN cases.

Another interesting observation from this study was that highest stability observed for fog generated with uncoated soot suggesting that chemical nature of FCN does play an important role in determining the fog characteristics. However, much more detailed study, including those focussing on fog droplet growth kinetics, morphological changes in nuclei, etc. needs to be carried out with this new facility in the near future.

ACKNOWLEDGMENTS

We acknowledge the financial support provided by Technology mission on Railway Safety (TMRS) Ministry of Railway and Ministry of Human Resource Development, Govt. of India and ICRS programme of DST. SNT acknowledges initial very useful discussion with K. Muralidhar.

REFERENCES

Amanna, A. (1999). *Virginia's Smart Road: A Transportation Research Facility Centre for Transportation Research*, Virginia tech, Blacksburg, USA.

Baumer, D., Vogelb, B., Versickb, S., Rinkeb, R., Mohlerb, O. and Schnaiterb, M. (2008). Relationship of Visibility, Aerosol Optical Thickness and Aerosol Size Distribution in an Ageing Air Mass over South-West Germany. *Atmos. Environ.* 42: 989–998.

Baumgardner, D., Dye, J., Gandrud, B. and Knollenberg, R. (1992). Interpretation of Measurements Made by the Forward Scattering Spectrometer Probe (FSSP-300) During the Airborne Arctic Stratospheric Expedition. *J. Geophys. Res.* 97: 8035–8046.

Baumgardner, D., Jonsso, H., Dawson, W., O' Connor, D. and Newton, R. (2001). The Cloud, Aerosol and Precipitation Spectrometer: A New Instrument for Cloud Investigations. *Atmos. Res.* 59: 251–264.

Bott, A. (1991). On the Influence of the Physico-Chemical Properties of Aerosols on the Life Cycle of Radiation Fog. *Boundary Layer Meteorol.* 55: 1–31.

Chate, D.M. and Devara, P.C.S. (2005). Growth Properties of submicron Aerosols during Cold Season in India. *Aerosol Air Qual. Res.* 5: 127–140.

Colomb, M., Hirech, K., Morange, P., Boreux, J.J., Lacote, P. and Dufour, J. (2008) An Innovative Artificial Fog Production Device Improved in the European Project "FOG". *Atmos. Res.* 87: 242–251.

Colomb, M., Hirech, K., Morange, P., Boreux, J.J., Lacote, P. and Dufour, J. (2004). Innovative Artificial Fog Production Device, a Technical Facility for Research Activities, Proceedings of the Third International Conference on Fog, Fog Collection and Dew, 11–15 Oct., Cape Town, South Africa, G4. p. 88–91.

Colomb, M., Serezat, L., Legoueix, G. and Boreux, J.J. (1999). Qualification of an Experimentation Centre to Test Visibility Conditions in Fog, Proceedings of the 8th International Conference on Vision in Vehicles. 22–25 August, Boston, USA.

Demokritou, P., Gupta, T., and Koutrakis, P. (2002). A High Volume Apparatus for the Condensational Growth of Ultrafine Particles for Inhalation Toxicological Studies. *Aerosol Sci. Technol.* 36: 1061–1072.

Fortner, B. (1999). High-tech Highway. *Civ. Eng.* 69: 38–41.

Frank, G., Martinsson, B.G., Cederfelt, S., Berg, O.H., Swietlicki, E. and Wendisch, M. (1998). Droplet Formation and Growth in Polluted Fogs. *Contrib. Atmos. Phys.* 71: 65–85.

Gerber, H.E. (1981). Microstructure of a Radiation Fog. *J. Atmos. Sci.* 38: 454–458.

Gupta, T., Demokritou, P. and Koutrakis, P. (2004). Effects of Physicochemical Properties of Ultrafine Particles on the Performance of an Ultrafine Particle Concentrator. *Aerosol Sci. Technol.* 38: 37–45.

Hansen., J.E. and Travis, L.D. (1974). Light Scattering in Planetary Atmospheres. *Space Sci. Rev.* 16: 527–610.

Hinds, W. (1999). *Aerosol Technology*, John Wiley & Sons Inc., New York.

Houghton, H.G. (1931). The Transmission of Visible Light through Fog. *Phys. Rev.* 38: 152–158.

Houghton, H.G. and Radford, W.H. (1938). On the Local Dissipation of Warm Fog. *Papers in Phys. Oceanogr. Meteorol.* 6: 63.

http://neuronresearch.net/vision/files/photopiceffic.htm.

http://www.wmo.ch/pages/prog/www/IMOP/publications/CIMO-Guide/Draft%207th%20edition/Part1-Ch09Final_Corr.pdf.

Hudson, J.G. (1980). Relationship between Fog Condensation Nuclei and Fog Microstructure. *J. Atmos. Sci.* 37: 1854–1867.

Kocmond, C.W., Garrett, W.D. and Mack, E.J. (1972).

Modification of Laboratory Fog with Organic Surface Films. *J. Geophys. Res.* 77: 3221–3231.

Mickey, A.J., Gonda, I., Irwin, W.J. and Flides, F.J.T. (1990). Effect of Hydrophobic Coating on the Behaviour of a Hygroscopic Aerosol Powder in an Environment of Controlled Temperature and Relative Humidity. *J. Pharm. Sci.* 79: 1009–1014.

Mohan, M. and Payra, S. (2009). Influence of Aerosol Spectrum and Air Pollutants on Fog Formation in Urban Environment of Megacity Delhi, India. *Environ. Monit. Assess.* 151: 265–277.

Nebuloni, R. (2005). Empirical Relationships between Extinction Coefficient and Visibility in Fog. *Appl. Opt.* 44: 3795–3804.

Pinnick, R.G., Hoihjelle, D.L., Fernandez, G., Stenmark, E.B., Lindberg, J.D. and Hoidale, G.B. (1978). Vertical Structure in Atmospheric Fog and Haze and its Effects on Visibility. *J. Atmos. Sci.* 35: 2020–2032.

Pruppacher, H. R. and Klett, J. D. (1997). *Microphysics of Clouds and Precipitation,* Reidel Publishing Company, Dordrecht-Holland.

PWRI (1988). *Development Testing Using Weather Environment Test Track*, Public Work Research Institute, Ministry of Construction.

Ruden, J.W., Wasser, C.F., Hulbert, S. and Burg, A. (1977). *Motorists Requirements for Active Grade Crossing Warning Devices*, Report No. FHWA-RD-77-167, U.S. Department of Transportation Federal Highway Administration, Washington, D.C.

Saathoff, H.; Mhler, O., Schurath, U., Kamm, S., Dippel B. and Mihelcic, D. (2003). The AIDA Soot Aerosol Characterization Campaign. *J. Aerosol Sci.* 34: 1277–1296.

Seinfeld, J.H. and Pandis, S.N. (2006). *Atmospheric Chemistry and Physics: from Air Pollution to Climate Change*, John Wiley and Sons, Inc., New York.

Varghese, S.K. and Gangamma, S. (2007). Evaporation of Water Droplets by Radiation: Effect of Absorbing Inclusions. *Aerosol Air Qual. Res.*7: 95–105.

Yuskiewicz, B.A., Orsini, D., Stratmann, F., Wendisch, M., Wiedensohler, A., Wobrock, W. and Schell, D. (1998). Changes in Submicrometer Particle Size Distributions and Light Scattering During Haze and Fog Events in a Highly Polluted Environment. *Biter. Phy. Atmos.* 71: 33–45.

Zhang, Z.Q. and Liu, B.Y.H. (1990). Dependence of the Performance of TSI 3020 Condensation Nucleus Counter on Pressure, Flow Rate, and Temperature. *Aerosol Sci. Technol*. 13: 493–504.

Received for review, August 22, 2010
Accepted, January 27, 2011